Biological Sciences: Neuroscience

Effects of the ecto-ATPase apyrase on microglial ramification and surveillance reflect cell depolarization not ATP depletion

Short title: Apyrase effects on microglia

Christian Madry[1,2,+], I. Lorena Arancibia-Cárcamo[1*], Vasiliki Kyrargyri[1*],

Victor T.T. Chan[1], Nicola Hamilton-Whitaker[1,3,+] and David Attwell[1,+]

[1]Department of Neuroscience, Physiology & Pharmacology,

University College London, Gower Street, London, WC1E 6BT, UK

[2]Institute of Neurophysiology, Charité - Universitätsmedizin, 10117, Berlin, Germany

[3]Wolfson Centre for Age Related Disease,

King's College London, Guy's Campus, London, SE1 1UL.

Corresponding author before publication:

David Attwell Tel: (+44)-20-7679-7342; Email: d.attwell@ucl.ac.uk

Corresponding author after publication:

David Attwell, Email: d.attwell@ucl.ac.uk

or Christian Madry, Email christian.madry@charite.de

or Nicola Hamilton-Whitaker Email: nicola.hamilton-whitaker@kcl.ac.uk

Abstract Microglia, the brain's innate immune cells, have highly motile processes which constantly survey the brain to detect infection, remove dying cells and prune synapses during brain development. ATP released by tissue damage is known to attract microglial processes, but it is controversial whether an ambient level of ATP is needed to promote constant microglial surveillance in the normal brain. Applying the ATPase apyrase, an enzyme which hydrolyses ATP and ADP, reduces microglial process ramification and surveillance, suggesting that ambient ATP/ADP maintains microglial surveillance. However, attempting to raise the level of ATP/ADP by blocking the endogenous ecto-ATPase (termed NTPDase1/CD39), which also hydrolyses ATP/ADP, does not affect the cells' ramification or surveillance, nor their membrane currents which respond to even small rises of extracellular [ATP] or [ADP] with the activation of K^+ channels. This indicates a lack of detectable ambient ATP/ADP and ecto-ATPase activity, contradicting the results with apyrase. We resolve this contradiction by demonstrating that contamination of commercially-available apyrase by a high K^+ concentration reduces ramification and surveillance by depolarising microglia. Exposure to the same K^+ concentration (without apyrase added) reduced ramification and surveillance as with apyrase. Dialysis of apyrase to remove K^+ retained its ATP-hydrolysing activity but abolished the microglial depolarisation and decrease of ramification produced by the undialysed enzyme. Thus, applying apyrase affects microglia by an action independent of ATP, and no ambient purinergic signalling is required to maintain microglial ramification and surveillance. These results also have implications for hundreds of prior studies that employed apyrase to hydrolyse ATP/ADP.

Key words: microglia, ATP, surveillance, apyrase

Significance statement

ATP mediates interactions between cells in many tissues, but is particularly important for microglia, the brain's immune cells, which constantly survey the brain to detect infection and to regulate the brain's wiring during development. It is controversial whether the ceaseless movement of microglia is driven by ATP release from brain cells. We show that an enzyme (apyrase) widely used to manipulate ATP levels is contaminated with K^+ ions which inhibit microglial surveillance, and that no ATP release is needed to drive microglial process movement. Thus, all conclusions about a role of ATP in signalling based on applying apyrase need re-examining, and brain immune surveillance is not regulated by ATP release.

\body **Introduction**

ATP-mediated signalling is present in many tissues, but is particularly important for microglia, the brain's innate immune cells (1). Microglia constantly survey the brain by extending and retracting their processes to sense their environment (2) but also, in the case of sudden brain damage, promptly send out processes to quickly target and enclose the site of injury (3). The latter response is mediated by ATP released from the damage site activating microglial $P2Y_{12}$ receptors (4, 5), but there is controversy over whether constant surveillance by microglia depends on activation of receptors by an ambient level of ATP or ADP in the extracellular solution. Understanding what drives surveillance is important because it enables microglia to detect brain damage or infection (6, 7) but also to monitor and modulate the functional state of synapses and neurons (8–10), to remove excessively generated synapses by pruning them during brain development (11, 12), and to regulate the number of neurons through phagocytic removal of surplus progenitor cells produced during development and adulthood (13, 14).

Several studies have reported that exposure to the ATP/ADP hydrolysing enzyme apyrase, both *in vivo* or in brain slices, evokes a rapid retraction of microglial processes and a reduction of surveillance (3, 15–17). This implies that a tonic extracellular purinergic signal may be needed to maintain microglial ramification and surveillance. Such a signal would imply a constant release of ATP into the extracellular space around microglial cells, and hydrolysis via ADP into AMP and adenosine by the activity of endogenous membrane-bound ecto-ATPases, such as the microglial-bound NTPDase-1/CD39 (18) and the less selectively expressed 5'-nucleotidase CD73 (reviewed in (19)). Since a rise of extracellular [ATP] acts as a potent danger signal in the brain, triggering a rapid immunological response, these ecto-ATPases maintain a very low extracellular ATP concentration, in the low nanomolar range (20–23). This low concentration is expected to be insufficient to activate even those purinergic receptors which display the highest affinity, such as the microglial ADP-preferring $P2Y_{12}$ subtype with an EC_{50} of ~100-200 nM (24). In agreement with this, recent reports show that microglial surveillance and ramification are independent of $P2Y_{12}$ receptor signalling (5, 25,

26), raising the question of how application of apyrase to lower extracellular nucleotide levels could affect microglial ramification and surveillance.

Apyrase, purified from potato or recombinant organisms (27) is an ecto-ATPase which hydrolyses a wide range of nucleotide (N) substrates including ATP and ADP, according to the general reaction: NTP → NDP + Pi → NMP + 2Pi. Ectopically applied apyrase is used widely to deplete endogenous nucleotides in biological preparations. Indeed, over 600 papers in PubMed report applying apyrase to perturb signalling mediated by extracellular ATP, on the assumption that this enzyme is acting by hydrolysing ATP and other nucleotides.

By using a combination of pharmacology, electrophysiology, ion-sensitive electrode measurements, protein dialysis, and two-photon and confocal microscopy of microglial cells, in acute hippocampal slices, we show that the apyrase-evoked reduction of microglial ramification and surveillance is not due to an abolition of tonic purinergic signalling. Instead, it is mediated by cell depolarisation produced by the high $[K^+]$ content of commercially-available apyrase. A similar depolarization produced by raising the extracellular $[K^+]$ ($[K^+]_e$) in the absence of apyrase has the same effects on ramification and surveillance, and dialysing out the contaminating K^+ abolishes the effect of apyrase while retaining its enzymatic activity. These results have important implications for our understanding of what drives microglial surveillance, but also for all experiments investigating purinergic signalling that employ apyrase to lower ATP levels.

Results

Apyrase decreases microglial ramification and surveillance

To test for an effect of putative tonic ATP-mediated signalling on microglial morphology, we exposed acutely-prepared P12 rat hippocampal slices to the ATP hydrolysing enzyme apyrase (200 U/ml, Sigma A7646 was used for all experiments except where indicated otherwise) for 30 min. After fixation of the tissue and immuno-labelling microglia for Iba-1, we quantified their process ramification by performing a 3-dimensional Sholl analysis. Individual microglial cells were analysed at a depth of at least 60 μm below the slice surface

(to avoid any effects due to slicing-evoked superficial cell damage) in high-resolution confocal image stacks. While untreated microglial cells (control) displayed a ramified morphology with a large number of long and highly branched processes (Fig. 1a), microglia exposed to apyrase had much shorter and less complex processes, covering a markedly reduced area than their untreated counterparts (Fig. 1b). The Sholl analysis showed that apyrase treatment reduced the number of intersections of microglial processes with concentric Sholl spheres at increasing distances from the soma (Fig. 1c), and reduced the number of branch points and process terminals (Fig. 1d, e).

To investigate how microglial surveillance is affected by apyrase exposure in real time, we imaged microglia in hippocampal slices using two-photon microscopy and quantified changes of baseline surveillance and ramification minute-by-minute (see Materials and Methods). Apyrase was locally applied to individual microglial cells through a pipette inserted into the tissue ~10-20 μm away from the cell's soma. This caused a rapid retraction of microglial processes (Fig. 1f) and decreased both the surveillance and ramification indices in a dose-dependent manner (Fig. 1g-j), whereas performing the same manipulation with extracellular solution in the pipette (Fig. 1g-h) had no effect (to allow local application of apyrase to raise its concentration around the cell significantly in this experiment, the rate of superfusion of extracellular solution was low, which is why the apyrase-evoked change does not reverse rapidly under these live imaging conditions, but recovery was seen using a different approach in Fig. 3m below). Thus, apyrase induces a strong and rapid loss of microglial processes, which would conventionally be interpreted as indicating the existence of a tonic extracellular purinergic signal maintaining microglial ramification and surveillance.

In order to test this hypothesis, we next assessed whether there is a detectable ATP concentration in the extracellular space of brain tissue, using ATP-evoked chemi-luminescence of firefly luciferase enzyme. This emits photons that can be detected with a photomultiplier (PMT), with a quantum yield of almost one photon per ATP molecule and a detection limit of <1 nM ATP (28, 29). Brief puffs (0.5 sec) of 1 mM ATP in extracellular solution produced a robust PMT-mediated current, which was greatly reduced in the presence of 100

U/ml apyrase (Fig. 1k, l), showing that added apyrase effectively hydrolyses extracellular ATP. However, when imaging the ATP-evoked signal from a hippocampal slice without any puffed ATP, we could not detect any difference in signal amplitude if the slice was removed (Fig. 1l, inset), implying (surprisingly, given the effect of apyrase described above) that the extracellular ATP concentration in slices is kept at a very low level, below the detection limit of this assay.

Lack of a tonic ATP release mechanism in baseline conditions

To further test whether extracellular ATP may be required to keep microglia motile and ramified, we next performed experiments interfering with ATP metabolism in brain tissue. Microglia express on their surface membrane high amounts of the ecto-ATPase NTPDase1/CD39 (18), which hydrolyses ATP or ADP into AMP which, in turn, is hydrolysed into adenosine by other types of ecto-enzyme (for review see (30)). This entire ecto-nucleotidase pathway operates very rapidly, with a half time for the conversion of ATP to adenosine of only ~200 msec (31). Thus, if there is an ambient level of ATP present around microglial cells then there needs to be a tonic release of ATP which will be constantly hydrolysed into ATP breakdown products. Consequently, blockade of ecto-ATPases should lead to an accumulation of extracellular ATP in slices (32). Microglia are very sensitive to increases of extracellular ATP concentration, to which they respond by activating $P2Y_{12}$ receptor-gated THIK-1 K^+ channels, generating an outward K^+ current which leads to a hyperpolarisation of their membrane (33). Puff-application of ATP (or ADP) to the slice surface caused a dose-dependent activation of this outward K^+ current in whole-cell voltage-clamped microglia held at 0 mV (Fig. 2a), which evoked a hyperpolarisation in unclamped cells (Fig. 2a, inset). Notably, even concentrations of ATP as low as 100 nM generated a clearly visible electrical response, emphasising that microglial cells can sense even a subtle rise of extracellular ATP concentration due to their expression of high affinity $P2Y_{12}$ receptors (5, 24).

Despite their sensitivity to ATP, the microglial resting membrane potential (Fig, 2b, c) and current (Fig. 2d, red dashed line) were not detectably affected by the application of 200 µM ARL-67156 (Fig. 2b-d), a widely used broad-spectrum NTPDase blocker (34, 35). Confirming that it did block endogenous ecto-ATPases however, ARL-67156 evoked a robust

~60% increase of the K^+ current evoked by brief puffs of ATP (Fig. 2d, e). This demonstrates that ARL-67156 effectively blocks the hydrolysis of exogenously applied ATP, thus potentiating its action, whereas no detectable turnover of ATP occurs in baseline conditions (Fig. 2b, c) suggesting that endogenous ATP levels are very low.

Any rise of extracellular ATP which might occur following ecto-ATPase block is also expected to induce changes of microglial surveillance and ramification (16, 36). To try to detect this, we imaged microglial motility by two-photon microscopy as in Fig. 1. Microglial cells were imaged at least 60 µm below the slice surface and exhibited a ramified morphology with highly motile processes showing constant extensions and retractions over time (Fig. 2f). After an initial 20 min control period we blocked ecto-ATPases by bath-applying 200µM ARL-67156. However, neither microglial surveillance nor ramification (Fig. 2g-j) were affected, again suggesting that the extracellular ATP concentration remained unaltered, and hence that little ATP is being released in the slice (in the absence of tissue damage).

In summary, chemiluminescence, electrophysiological and imaging experiments exclude the existence of a baseline extracellular ATP concentration high enough to drive microglial purinergic signalling. Thus, the apyrase-evoked decrease of microglial surveillance and ramification is unlikely to reflect hydrolysis of extracellular ATP.

Apyrase depolarises microglia due to its high K^+ content

We have recently shown that microglial surveillance and ramification are regulated by the cell's resting membrane voltage, which is set by the tonic activity of its K^+ channels, such that pharmacological block or knock-out of the main microglial K^+ channel (THIK-1) evokes depolarisation of the cell and a loss of ramification and surveillance (33). Surprisingly, application of apyrase to hippocampal slices evoked a strong and reversible dose-dependent depolarisation of current-clamped microglial cells (Fig. 3a, b). In some experiments, to prevent any putative purinergic signalling between microglia and their surrounding cells, we carefully lifted the whole-cell patch-clamped cell out of the slice while maintaining the whole-cell configuration (Fig. 3c). After isolating the cell from its native environment we confirmed that it still responded to brief puffs of ATP by generating outward K^+ currents (Fig. 3c). Exposure to

apyrase evoked an inward membrane current at a holding potential of 0mV (Fig. 3c, arrow) which we will show below results from a rise in $[K^+]_e$ decreasing K^+ efflux occurring at 0 mV through tonically active potassium channels. Apyrase also diminished the ATP-evoked outward K^+ current, which could reflect both a decrease in the driving force for K^+ efflux and apyrase hydrolysing some of the puff-applied ATP (Fig. 3c). A detailed analysis of the effects apyrase has on the electrophysiology of microglia is given in the Supporting Information (Fig. S1).

To test the idea that apyrase raises the extracellular $[K^+]$, we measured $[K^+]_e$ using K^+-sensitive electrodes inserted into the slice. Indeed, application of apyrase to slices led to a dramatic rise of $[K^+]_e$ (Fig. 3d), which was dose-dependent and did not require a slice to be present at all (Fig. 3e). Thus, the apyrase solution contained, apart from the actual enzyme, also high amounts of potassium. The apyrase that we tested in most of our experiments is a very commonly used type (catalogue number A7646) from Sigma, the largest supplier with the greatest varieties of different apyrase preparations extracted either from potato (the majority) or recombinantly expressed. A literature search revealed that the vast majority of researchers obtained apyrase from Sigma, most commonly the preparations A6132, A6410, A6535 and A7646 which vary in the apyrase units/(mg protein) and purification grades. We therefore compared the resulting potassium concentrations of 6 different and frequently used apyrase preparations made up at 100 U/ml each (in standard extracellular solution containing 2.5 mM $[K^+]$ in the absence of apyrase: see Materials and Methods) using a commercial blood gas analyser. All preparations had significantly elevated $[K^+]$ contents, which correlated roughly inversely with the number of units of enzyme per mg of solid preparation (Fig. 3f, g). In the case of two apyrase types (A6132 and A6237) $[K^+]_e$ reached extremely high concentrations in the range of 30-40 mM $[K^+]$, even at 100 U/ml, a concentration frequently used in published experiments in tissue slices or *in vivo* (100-500 U/ml).

Next we tested the effect of an elevated potassium concentration (raised by 20 mM, to a total of 22.5 mM, with $[Na^+]$ lowered correspondingly) on microglial morphology in the absence of any apyrase, using Sholl analysis as in Fig. 1. A 30 min exposure of slices to 22.5

mM [K^+], which roughly equates to the [K^+] present in the slices in 200 U/ml apyrase (A7646) (Fig. 3d, e), caused a severe de-ramification of microglial cells (Fig. 3h-j) with a strong reduction in the number of branch points and terminal processes (Fig. 3k, l). The morphology in high $[K^+]_e$ almost exactly matched that seen with apyrase treatment as shown in Fig. 1, and led to a reduced rate of surveillance of the brain because of the smaller number of processes. The time course of the onset of the deramification, and of the recovery when apyrase or elevated $[K^+]_e$ was removed, were not significantly different (Fig. 3m, 2-way ANOVA p=0.68). Thus, apyrase induces morphological changes in microglia by virtue of the high $[K^+]_e$ it contains, and not via ATP depletion.

Dialysing apyrase retains enzyme activity but abolishes effects on microglial ramification and hence surveillance

To test whether there is any tonic purinergic signalling affecting microglial properties, which may have been masked by the high [K^+] content present in the apyrase preparations, we removed the high [K^+] by dialysis against normal extracellular solution. Using a dialysis membrane with a cut-off molecular weight of 2 kDa, salts and other small molecules below this threshold were removed, while apyrase with a molecular weight of ~45kDa was retained.

We first verified that the dialysed apyrase depleted [ATP] as effectively as the non-dialysed apyrase from the same batch by measuring chemiluminescence-derived signals as in Fig. 1k. As with the non-dialysed enzyme, dialysed apyrase greatly reduced the luciferase signal evoked by an ATP puff (Fig. 4a), showing that dialysis did not affect the enzymatic activity of the apyrase. However, 200 U/ml dialysed apyrase had no effect on the resting membrane potential (Fig. 4b) and did not alter the membrane current of the microglia (Fig. S2a-b), while the same batch of non-dialysed apyrase depolarised the cells (Fig. 4b), evoked an inward membrane current at 0 mV, and increased the cells' conductance at negative potentials (Fig. S2a-b; see Supporting Information for detailed analysis). This clearly demonstrates that [K^+] has been effectively removed from the apyrase preparation and furthermore indicates that no tonic ATP levels are present and necessary to maintain the resting potential of microglial cells.

Finally, we investigated the effect of dialysed apyrase, which should lower the extracellular ATP concentration without raising $[K^+]_e$, on microglial morphology, using Sholl analysis. Strikingly, microglial cells remained as ramified as under untreated control conditions when exposed to 200 U/ml dialysed apyrase (Fig. 4c, d, f), while 200 U/ml of the non-dialysed enzyme induced the expected decrease in process ramification (Fig. 4e-f). Thus, all the effects of undialysed apyrase on microglial ramification, and hence on surveillance which is reduced when there are less processes, are produced by the high $[K^+]$ present in this product and not by ATP depletion.

Discussion

Microglial ramification and process movement are critical for normal brain function, since they underpin the ability of these cells to constantly survey the brain. This surveillance is thought to allow the cells not only to detect invading microorganisms, but also to prune redundant synapses during development and to regulate neuronal activity. It has been suggested that microglial surveillance may require tonic ATP-evoked signalling in microglia, in part on the basis of experiments lowering the extracellular ATP concentration by applying the ATPase apyrase, which we now show is contaminated by K^+ ions which will depolarise the microglia. Using dialysed, purified apyrase allowed us to investigate the role of endogenous nucleotides in regulating microglial surveillance and morphology, without a superimposed elevation of external $[K^+]$ which may generate effects independent of purinergic signalling.

Our findings show that microglial cells do not receive any tonic purinergic input that is required to maintain their morphology and constant surveillance in the healthy brain. Surprisingly, the reduced ramification and surveillance evoked by apyrase that we and others have observed are not due to its enzymatic activity, but are produced by the high $[K^+]$ content present in commercially-available apyrase preparations, which causes a significant depolarisation of the cells. We have recently shown that such a depolarisation is sufficient to dramatically reduce microglial ramification and surveillance, which are regulated and maintained by the cell's resting potential, which is set by the tonic activity of the cells' K^+

channels (33). Fig. 3h-m shows the direct effect of depolarisation by high $[K^+]_e$ on hippocampal microglial morphology (since microglia may vary in their properties according to brain region (37), the magnitude of the effect of depolarisation on microglial morphology may vary between brain regions). The rise of $[K^+]_e$ to ~60 mM that occurs during the spreading depression associated with migraine, stroke, sub-arachnoid haemorrhage or brain injury (38), or the anoxic depolarisation induced by ischaemia (39), and the 10 mM $[K^+]_e$ rise occurring during synchronous high frequency activity of neurons in epilepsy (39), are expected to depolarise microglia and decrease their ramification and surveillance. In contrast, the $[K^+]_e$ rise occurring during normal neuronal activity (~1 mM: 39) is much smaller and will have little effect.

Non-activated microglial cells selectively express G_i-protein coupled $P2Y_{12}$ receptors (5, 40), which exhibit a very high affinity for adenosine nucleotides, with an EC_{50} value for ADP in the range of ~100 nM (24). In addition, these receptors are linked to the activation of microglial K^+ channels (33), hence making the $P2Y_{12}$-K^+ channel signalling complex an ideal sensor to translate even subtle rises of ATP or ADP concentration into an electrical signal or other downstream messengers. It was not surprising, then, that several studies reported that microglial morphology and surveillance are regulated by a tonic purinergic input that is essential for keeping the cells ramified and motile. These conclusions were obtained (see Fig. 5) by applying exogenous apyrase (3, 15–17), or knocking out the endogenous ecto-ATPase (NTPDase1/CD39) (18, 41), in order to manipulate the extracellular nucleotide levels produced by any tonic nucleotide release that does occur. However, our results show that non-activated microglia receive no tonic purinergic input to maintain their ramification and surveillance, since application of dialysed, $[K^+]$-free apyrase evoked neither a change of their membrane currents nor of their morphology, indicating a lack of a tonic activation of microglial purinergic receptors. Consistent with our results, experiments with $P2Y_{12}$ receptors blocked or knocked out, which abolished microglial process outgrowth in response to a sudden rise of $[ATP]_e$, had no effect on microglial surveillance, ramification or membrane potential (5, 25, 26, 33).

Since a rise of extracellular nucleotides is recognised as a potent danger signal by microglia, tonic levels of ATP or ADP are normally kept very low (21–23, 42–44) and our data suggest that they are not sufficient to tonically activate $P2Y_{12}$ receptors. Only when extracellular [ATP] and [ADP] rise significantly, e.g. due to brain damage, are $P2Y_{12}$ receptors effectively activated, in order to mediate rapid process extension to the site of injury (ATP leakage). This targeted motility depends on ecto-ATPases, since their inhibition with ARL-67156 abolishes the outgrowth of microglial processes to an ATP source (36, 45). This may involve the generation of ADP from ATP, to activate $P2Y_{12}$ receptors, but could also involve ecto-ATPase mediated generation of adenosine which acts on microglial A_3-type adenosine receptors (41, 45, 46). Thus, ecto-ATPase regulation of extracellular nucleotide levels is important for targeted microglial motility evoked by a rise of extracellular ATP levels, but whether ecto-ATPases also contribute to microglial physiology in resting conditions, in the absence of any brain damage-derived ATP release, is more controversial.

Our results show that blocking ecto-ATPases (with ARL-67156) in resting conditions caused no changes of microglial ramification and surveillance, and did not evoke a $P2Y_{12}$ receptor-evoked electrical response in patch-clamped microglial cells. In contrast to our finding, Matyash et al. (41) have found that microglial cells were less ramified when NTPDase1 (CD39) is knocked out, suggesting that constitutive ATP/ADP breakdown by NTPDase1 and tonic activity of $P2Y_{12}$ and adenosine receptors are required to maintain a ramified microglial morphology. However, in these studies NTPDase1 was globally knocked-out and the effects on microglial morphology of a direct, pharmacological inhibition or microglial-specific knock-out were not tested. This is important, since NTPDase1-mediated effects can also originate from other cells (47). NTPDase1 is also prominently expressed at the surface of vascular smooth muscle cells (18, 40), where it contributes to the regulation of vascular tone and modulates vascular inflammation and thrombosis (48–50). Since microglial cells are in constant, bi-directional communication with blood vessels and endothelial cells (51, 52), the less ramified morphology observed in NTPDase1 KO animals may be the result of a primed or chronically activated phenotype originating from an altered micro-environment around blood

vessels. Furthermore, NTPDase1 exhibits functions beyond its enzymatic activity by interacting with Ran Binding Protein M (RanBPM) through its cytoplasmic N-terminal domain (53). RanBPM is ubiquitously expressed in the brain and acts as an intracellular signalling hub for a variety of signalling proteins including surface β-integrins (54), which regulate microglial morphology and process dynamics (55, 56). Conceivably, knock-out of NTPDase1 may cause microglial de-ramification by interrupting RanBPM-signalling, independent of any changes in purinergic signalling. Further evidence for a lack of tonic ATP release and NTPDase1 activity under physiological conditions is the finding that extracellular adenosine levels are not generated by NTPDase-mediated ATP hydrolysis, but mainly result from a direct release of adenosine from cells (57).

A key outcome of our study is that, surprisingly, all apyrase preparations that we tested, which are commonly used by researchers, were contaminated by a high [K^+] content, which presumably arises from the process by which the apyrase is manufactured. Sigma-Aldrich is by far the most popular supplier of apyrase preparations for scientists. A *Google scholar* search using the search terms “apyrase Axxxx” revealed the following number of publications for different Sigma-Aldrich apyrase types: A6132 – 68, A6535 – 97, A7646 – 33, A6410 – 58 (though most publications list only the supplier’s name without the catalogue number). In experiments performed on brain slices and *in vivo*, apyrase is commonly used at concentrations of 100-300 U/ml (500 U/ml is the maximum), which corresponds to a rise of extracellular [K^+] in the range of 5 to >80mM.

Apyrase is commonly used in neurobiological studies due to the widespread role of ATP as a neurotransmitter (58). Using the search terms “apyrase neuron” in NCBI/PubMed results in 111 publications, whereas “apyrase glia” gives 83 hits, of which the majority studied astrocytes (57 papers) and microglia (27 papers). For instance, in the astrocyte field, apyrase has been used in brain slices, retinal explants (*ex vivo*) or *in vivo* at higher doses between 25-300 U/ml to investigate the ATP dependence of astroglial calcium signalling (59, 60), the mechanisms of ATP release from astrocytes (61–63), or astrocyte-neuron communication (64–66). Similarly for microglia, apyrase-induced depletion of extracellular purines in brain

slices or *in vivo* has been used to investigate the role of extracellular ATP in (i) microglial baseline surveillance and targeted motility to focal tissue damage or an ATP source (3, 15–17, 25, 62, 67–69), (ii) microglial-astrocyte communication (3, 60, 70), (iii) ischaemia-induced microglial death (71) and (iv) hypotonia-evoked microglial ATP release (72). Without questioning the conclusions of these studies, which usually reflect evidence from a number of different experimental approaches, the fact that undialysed apyrase can strongly depolarise cells due to its accompanying [K^+] content makes it essential to re-assess some of the results obtained, particularly from experiments using a higher dose of apyrase. Protein dialysis provides a simple and effective way to remove the unwanted K^+ from apyrase while retaining its enzymatic activity, and we strongly advocate this procedure for any further studies using apyrase.

In conclusion, our study demonstrates that the extracellular ATP concentration in healthy brain tissue is not sufficient to drive tonic purinergic signalling in microglia, which is hence not required to maintain their surveillance and ramification under non-activated “resting” conditions.

Materials and Methods

Brain slice preparation

Animal procedures were carried out in accordance with the guidelines of the UK Animals (Scientific Procedures) Act 1986 and subsequent amendments. Acute hippocampal slices (300 µm thick, see schematic in Fig. 1k) were prepared (73) from P12 Sprague-Dawley rats of either sex, in ice-cold solution containing (mM) 124 NaCl, 26 $NaHCO_3$, 1 NaH_2PO_4, 2.5 KCl, 2 $MgCl_2$, 2 $CaCl_2$, 10 glucose, bubbled with 95% O_2/5% CO_2, pH 7.4, as well as 1 mM Na-kynurenate to block glutamate receptors. Brain slicing does not activate microglia for at least 4 hours, as judged by cell morphology, motility and interleukin 1β release (74, 75), and allows pharmacological investigation of mechanisms in a manner that is not possible using *in vivo* experiments. Supporting this, surveillance and ramification of microglia were essentially constant during imaging for up to an hour in brain slices (Fig. 3D of ref. 33; Fig. 1g-h) while in contrast the microglia would retract their processes and decrease surveillance if they were becoming activated. Slices were incubated for 30 min in darkness at room temperature (22–24°C) in oxygenated HEPES-buffered external solution (see below) containing 25 µg/ml Alexa 594 conjugated isolectin B_4 (ThermoFisher) for all experiments involving live imaging or 25 µg/ml Alexa 568 conjugated isolectin B_4 for electrophysiology experiments (74, 76), before being used in experiments. Isolectin B_4 labelling does not activate microglia (76) and its use avoids functional changes which might occur in transgenically-labelled microglia.

Solutions and electrophysiology

Slices were superfused with HEPES-buffered solution, at 34-36^oC for all experiments involving imaging and at room temperature (22-24^oC) for electrophysiological experiments, containing (mM) 140 NaCl, 2.5 KCl, 10 HEPES, 1 NaH_2PO_4, 2 $CaCl_2$, 1 $MgCl_2$, 10 glucose, pH set to 7.4 with NaOH, bubbled with 100% O_2. When the [KCl] was raised by 20 mM, [NaCl] was lowered by 20 mM. Cells were whole-cell clamped with electrodes containing KCl based solution, comprising (mM) 125 KCl (or CsCl), 4 NaCl, 1 $CaCl_2$, 10 HEPES, 10 EGTA, 4 MgATP, 0.5 Na_2GTP, pH set to 7.1 with KOH or CsOH. The final osmolarity was 285±5 mOsmol/kg. Microglia were identified by their fluorescent label and ramified morphology, and

whole-cell clamped at a depth of ~50-100 µm in the slice using borosilicate pipettes with a tip resistance of ~4-5 MΩ, giving a series resistance of <20 MΩ. Electrode junction potentials were compensated. I-V relations were from responses to 200 msec voltage steps ranging from -120 mV to +60 mV in 30 mV increments. Voltage- and current-clamp recordings were performed using a MultiClamp 700B amplifier (Molecular Devices). Currents were filtered at 1 kHz, digitized (10 kHz) and analysed off-line using pClamp10 software.

Drugs and dialysis

Drugs were obtained from Sigma-Aldrich or Tocris, and in live-imaging or electrophysiological experiments were applied via the bath perfusion (ARL-67156, $BaCl_2$) or locally via pressure ejection from a puffing pipette placed at the slice surface (in the case of ATP). Apyrase was applied either directly as a bolus to the perfusion chamber with the flow temporarily stopped (in electrophysiological experiments) or added to a patch pipette inserted into the slice tissue and puffed onto an individual microglial cell that was real-time imaged (Fig. 1f-j).

Dialysis of apyrase was performed using a 3 ml dialysis cassette (Slide-A—Lyzer, Thermo Scientific, 2 kDa MWCO, Cat. No. 87718) placed in cold dialysis buffer (HEPES-buffered extracellular solution) with 300x the sample volume for 2 hours at 4°C. The dialysis buffer was stirred and changed after 1 hour.

Chemiluminescence assay

ATP was measured with a luciferin/luciferase-based chemiluminescence assay which is specific for the detection of ATP. Superfusion of brain slices was halted and aliquots containing 25 µl of luciferin stock (Sigma L9506; 12 mg/ml in extracellular solution) and 25 µl of luciferase stock (Applichem A1006; 6 mg/ml in 0.5 M Tris buffer, pH 7.5) were added to a total bath chamber volume of ~0.5 ml at room temperature (as luciferase is not stable at higher temperatures). ATP-derived bioluminescence was detected using a photomultiplier tube (Thorn EMI Electronics 9224B, input voltage set to 1000 V) in darkness. This system is able to detect 6.2×10^{-11} M ATP (29). Photo-electrical currents were amplified, digitized and recorded using pClamp10.

Potassium measurements

Measurements of $[K^+]_e$ in experiments on brain slices were performed using custom-made potassium-sensitive electrodes fabricated and calibrated as described (77).

The $[K^+]$ in extracellular solution (without a slice) to which different apyrase preparations were added (at 100 U/ml) was also measured using a blood-gas analyser (Siemens RapidLab 348EX) set to dialysis mode. The inbuilt potassium sensor was calibrated according to the manufacturer's instructions and measurements were interleaved with control extracellular solution containing a preset potassium concentration. Values in Fig. 3f refer to the total $[K^+]$ including the 2.5 mM KCl of the standard extracellular solution.

Two-photon imaging

Microglia in hippocampal slices were imaged at 34-36^{o}C, at a depth of ~50-100 µm in the slice (to avoid studying superficial microglia that had started to become activated by the slicing procedure) using a Zeiss LSM 710 microscope (with a 20X lens, NA 1.0) and a Spectraphysics Mai Tai DeepSee eHP Ti:sapphire infrared laser. For imaging of microglia labelled with isolectin B_4-Alexa 594, the laser was tuned to a wavelength of 800 nm; generally the laser was adjusted to 1.8-2% of its maximum power, corresponding to ~5 mW at the preparation. The pixel dwell time was 1 µsec. For imaging of microglial surveillance, stacks of 21-31 slices imaged at 2 µm depth intervals were acquired every 60 sec. Images were typically 512 by 512 pixels and covered a square field of view 200 to 250 µm wide.

Image analysis

Analysis of two-photon images was performed using custom-written ImageJ (NIH) and MATLAB scripts (The MathWorks, Inc.), available at https://github.com/AttwellLab/Microglia. For analysis and quantification of microglial surveillance, each slice of every stack was filtered with a median filter after subtraction of smooth continuous background with the ImageJ 'subtract background' plugin with a ball size of 30 pixels. The 4D stacks were then registered first for lateral drift, then rotated 90° on their side, registered for z-drift and rotated back to their original orientation. We then performed a maximum intensity projection. Cells of interest were individually selected by manually drawing a region of interest (ROI) around an area including

all their process extensions over the whole duration of the resulting 2D movie, and erasing data around that ROI. These 2D movies of individual cells were then manually binarised and saved as independent files.

To quantify surveillance, for each movie, starting with the second frame, we subtracted from each binarised frame F_t the preceding frame F_{t-1} and created two binarised movies, *PE* consisting of only the pixels containing process extensions (F_t-$F_{t-1} > 0$) and *PR* consisting of only the pixels containing process retractions (F_t-$F_{t-1} < 0$). In both *PE* and *PR*, all other pixels are set to 0. The baseline surveillance index *B* is defined as the sum over all non-zero pixels in *PE* + *PR* normalised by its average over the initial 20 minutes of each experiment, i.e.:

$$B = (\Sigma_{pixels}\ PE+PR)/<(\Sigma_{pixels}\ PE+PR)>_{control}$$

where Σ_{pixels} denotes a sum taken over all non-zero pixels and $< >_{control}$ denotes a temporal average taken over the control period of the experiment (the first twenty minutes here). Surveillance indices were calculated as absolute values according to $B = (\Sigma_{pixels}\ PE+PR)$, and subsequently normalised to the control condition. The surveillance index provides a measure of the brain volume that is surveyed by a microglial cell in a given time. It is affected both by the rate at which processes elongate and shorten, and by the overall number of the microglial processes and their length.

To quantify ramification, in each movie frame, the MATLAB functions bwarea (uk.mathworks.com/help/images/ref/bwarea.html) and bwperim with 8-connected neighbourhood (uk.mathworks.com/help/images/ref/bwperim.html) were used to quantify respectively the area and the perimeter of the cell. The ramification index *R* is defined as the ratio of the perimeter to the area, normalised by that same ratio calculated for a circle of the same area. Specifically:

$$R = (\text{perimeter}/\text{area}) / [2.(\pi/\text{area})^{1/2}].$$

Thus, $R = 1$ if the cell is a perfect circle. The more ramified the cell, the larger *R* is. In 134 cells in hippocampal slices the mean value of *R* was 6.44±0.14 at the beginning of the experiment.

Sholl analysis

Microglial morphology was also assessed by Sholl analysis (78). Rat hippocampal brain slices were prepared as described above. After a 30 min recovery, slices were incubated at room temperature in oxygenated extracellular solution containing 100 or 200 U/ml apyrase (A7646) or 22.5 mM $[K^+]_e$ for 30 mins (for Figs. 1a-e and 3j-l) or (for Fig. 3m) for 7.5 and 15 mins followed by a further 15 mins in solution without added apyrase or 22.5 mM $[K^+]_e$ to observe recovery from the effects of apyrase and K^+. Tissue sections were then fixed in 4% paraformaldehyde for 45 minutes. After washing 3 times for 15 mins in PBS slices were blocked and permeabilized in 10% normal goat serum and 0.25% Triton X-100 in PBS for 4 hours at room temperature and then incubated at 4°C overnight in rabbit anti-Iba1 (Synaptic Systems, Cat. No. 234003, at 1:500) antibody prepared in blocking solution. After washing 3 times for 20mins in PBS, slices were incubated overnight in secondary antibody (goat anti-rabbit Alexa 543, Invitrogen, at 1:500). Slices were then washed in PBS, incubated in DAPI (Invitrogen) and mounted on glass slides using DAKO fluorescence mounting medium. Z-stacks of individual microglial cells located at ~60 µm below the slice surface were acquired at 0.3 µm depth intervals using a 63X oil immersion objective (NA 1.4) on a Zeiss LSM700 confocal microscope. Image stacks were pre-processed in ImageJ by median filtering ('despeckling') after subtraction of smooth continuous background with a ball size of 30 pixels and saved as TIF files. Reconstructions of individual microglial cells were carried out using 3D automatic cell tracing in Vaa3D software (www.vaa3d.org). Morphological parameters were then extracted using custom code written in MATLAB. The software used is available at https://github.com/AttwellLab/Microglia.

Statistics

Data are presented as mean±s.e.m. P values are from two tailed Student's t-tests (for normally distributed data) or Mann-Whitney U tests (for non-normally distributed data). Normality of data was checked using the Kolmogorov-Smirnov or Shapiro-Wilk test and equality of variance confirmed using the F-test. Sholl analysis distributions were compared with a Kolmogorov-Smirnov test. For multiple comparisons, p values are corrected using a

procedure equivalent to the Holm-Bonferroni method (for N comparisons, the most significant p value is multiplied by N, the 2nd most significant by N-1, the 3rd most significant by N-2, etc.; corrected p values are significant if they are less than 0.05).

Acknowledgements Supported by the Wellcome Trust (099222/Z/12/Z) and the European Research Council (BrainEnergy). We thank Renaud Jolivet for discussion and software.

References

1. Madry C, Attwell D (2015) Receptors, ion channels, and signaling mechanisms underlying microglial dynamics. J Biol Chem 290(20):12443–12450.
2. Nimmerjahn A (2005) Resting microglial cells are highly dynamic surveillants of brain parenchyma in vivo. *Science* 308(5726):1314–1318.
3. Davalos D, et al. (2005) ATP mediates rapid microglial response to local brain injury in vivo. *Nat Neurosci* 8(6):752–758.
4. Honda S, et al. (2001) Extracellular ATP or ADP induce chemotaxis of cultured microglia through Gi/o-coupled P2Y receptors. *J Neurosci* 21(6):1975–1982.
5. Haynes SE, et al. (2006) The $P2Y_{12}$ receptor regulates microglial activation by extracellular nucleotides. *Nat Neurosci* 9(12):1512–1519.
6. Prinz M, Priller J (2014) Microglia and brain macrophages in the molecular age: from origin to neuropsychiatric disease. *Nat Rev Neurosci* 15(5):300–312.
7. Wolf SA, Boddeke HWGM, Kettenmann H (2017) Microglia in physiology and disease. *Annu Rev Physiol* 79(1):619–643.
8. Wake H, Moorhouse AJ, Jinno S, Kohsaka S, Nabekura J (2009) Resting microglia directly monitor the functional state of synapses in vivo and determine the fate of ischemic terminals. *J Neurosci* 29(13):3974–3980.
9. Tremblay M-È, Lowery RL, Majewska AK (2010) Microglial interactions with synapses are modulated by visual experience. *PLoS Biol* 8(11):e1000527.
10. Li Y, Du X, Liu C, Wen Z, Du J (2012) Reciprocal regulation between resting microglial dynamics and neuronal activity in vivo. *Dev Cell* 23(6):1189–1202.
11. Paolicelli RC, et al. (2011) Synaptic pruning by microglia is necessary for normal brain development. *Science* 333(6048):1456–1458.
12. Schafer DP, et al. (2012) Microglia sculpt postnatal neural circuits in an activity and complement-dependent manner. *Neuron* 74(4):691–705.
13. Marín-Teva JL, et al. (2004) Microglia promote the death of developing Purkinje cells. *Neuron* 41(4):535–547.

14. Sierra A, et al. (2010) Microglia shape adult hippocampal neurogenesis through apoptosis-coupled phagocytosis. *Cell Stem Cell* 7(4):483–495.
15. Kurpius D, Nolley EP, Dailey ME (2007) Purines induce directed migration and rapid homing of microglia to injured pyramidal neurons in developing hippocampus. *Glia* 55(8):873–884.
16. Fontainhas AM, et al. (2011) Microglial morphology and dynamic behavior is regulated by ionotropic glutamatergic and GABAergic neurotransmission. *PLoS ONE* 6(1):e15973.
17. Eyo U, Dailey ME (2012) Effects of oxygen-glucose deprivation on microglial mobility and viability in developing mouse hippocampal tissues. *Glia* 60(11):1747-1760.
18. Braun N, et al. (2000) Assignment of ecto-nucleoside triphosphate diphosphohydrolase-1/cd39 expression to microglia and vasculature of the brain. *Eur J Neurosci* 12(12):4357–4366.
19. Zimmermann H (2000) Extracellular metabolism of ATP and other nucleotides. *Naunyn Schmiedebergs Arch Pharmacol* 362(4–5):299–309.
20. Joseph SM, Buchakjian MR, Dubyak GR (2003) Colocalization of ATP release sites and ecto-ATPase activity at the extracellular surface of human astrocytes. *J Biol Chem* 278(26):23331–23342.
21. Melani A, et al. (2005) ATP extracellular concentrations are increased in the rat striatum during in vivo ischemia. *Neurochem Int* 47(6):442–448.
22. Wall MJ, Atterbury A, Dale N (2007) Control of basal extracellular adenosine concentration in rat cerebellum. *J Physiol* 582(Pt 1):137–151.
23. Heinrich A, Andó R, Túri G, Rózsa B, Sperlágh B (2012) K^+ depolarization evokes ATP, adenosine and glutamate release from glia in rat hippocampus: a microelectrode biosensor study. *Br J Pharmacol* 167(5):1003–1020.
24. Abbracchio MP, et al. (2006) International Union of Pharmacology LVIII: update on the P2Y G protein-coupled nucleotide receptors: from molecular mechanisms and pathophysiology to therapy. *Pharmacol Rev* 58(3):281–341.

25. Sieger D, Moritz C, Ziegenhals T, Prykhozhij S, Peri F (2012) Long-range Ca^{2+} waves transmit brain-damage signals to microglia. *Dev Cell*. 22(6):1138-1148.
26. Sipe GO, et al. (2016) Microglial $P2Y_{12}$ is necessary for synaptic plasticity in mouse visual cortex. *Nat Commun* 7:10905.
27. Handa M, Guidotti G (1996) Purification and cloning of a soluble ATP-diphosphohydrolase (apyrase) from potato tubers (Solanum tuberosum). *Biochem Biophys Res Commun* 218(3):916–923.
28. Seliger HH, McElroy WD (1960) Spectral emission and quantum yield of firefly bioluminescence. *Arch Biochem Biophys* 88:136–141.
29. Wieraszko A, Goldsmith G, Seyfried TN (1989) Stimulation-dependent release of adenosine triphosphate from hippocampal slices. *Brain Res* 485(2):244–250.
30. Zimmermann H, Zebisch M, Sträter N (2012) Cellular function and molecular structure of ecto-nucleotidases. *Purinergic Signal* 8(3):437–502.
31. Dunwiddie TV, Diao L, Proctor WR (1997) Adenine nucleotides undergo rapid, quantitative conversion to adenosine in the extracellular space in rat hippocampus. *J Neurosci* 17(20):7673–7682.
32. Wall MJ, Dale N (2007) Auto-inhibition of rat parallel fibre–Purkinje cell synapses by activity-dependent adenosine release. *J Physiol* 581(2):553–565.
33. Madry C, et al. (2018) Microglial ramification, surveillance and interleukin 1β release are regulated by the two-pore domain K^+ channel THIK-1. *Neuron* **97**, 1-14. https://doi.org/10.1016/j.neuron.2017.12.002
34. Iqbal J, Vollmayer P, Braun N, Zimmermann H, Müller CE (2005) A capillary electrophoresis method for the characterization of ecto-nucleoside triphosphate diphosphohydrolases (NTPDases) and the analysis of inhibitors by in-capillary enzymatic microreaction. *Purinergic Signal* 1(4):349–358.
35. Lévesque SA, Lavoie ÉG, Lecka J, Bigonnesse F, Sévigny J (2007) Specificity of the ecto-ATPase inhibitor ARL 67156 on human and mouse ectonucleotidases. *Br J Pharmacol* 152(1):141–150.

36. Dissing-Olesen L, et al. (2014) Activation of neuronal NMDA receptors triggers transient ATP-mediated microglial process outgrowth. *J Neurosci* 34(32):10511–10527.

37. De Biase LM et al. (2017) Local cues establish and maintain region-specific phenotypes of basal ganglia microglia. *Neuron* **95**, 341-356.

38. Lauritzen M et al. (2011) Clinical relevance of cortical spreading depression in neurological disorders: migraine, malignant stroke, subarachnoid and intracranial hemorrhage, and traumatic brain injury. *J Cereb Blood Flow Metab* **31**, 17-35.

39. Hansen AJ (1985) Effect of anoxia on ion distribution in the brain. *Physiol Rev* **65**, 101-148.

40. Zhang Y, et al. (2014) An RNA-sequencing transcriptome and splicing database of glia, neurons, and vascular cells of the cerebral cortex. *J Neurosci* 34(36):11929–11947.

41. Matyash M, Zabiegalov O, Wendt S, Matyash V, Kettenmann H (2017) The adenosine generating enzymes CD39/CD73 control microglial processes ramification in the mouse brain. *PLOS ONE* 12(4):e0175012.

42. Hamann M, Attwell D (1996) Non-synaptic release of ATP by electrical stimulation in slices of rat hippocampus, cerebellum and habenula. *Eur J Neurosci* 8(7):1510–1515.

43. Joseph SM, Buchakjian MR, Dubyak GR (2003) Colocalization of ATP release sites and ecto-ATPase activity at the extracellular surface of human astrocytes. *J Biol Chem* 278(26):23331–23342.

44. Frenguelli BG, Wigmore G, Llaudet E, Dale N (2007) Temporal and mechanistic dissociation of ATP and adenosine release during ischaemia in the mammalian hippocampus. *J Neurochem* 101(5):1400–1413.

45. Färber K, et al. (2008) The ectonucleotidase cd39/ENTPDase1 modulates purinergic-mediated microglial migration. *Glia* 56(3):331–341.

46. Ohsawa K, et al. (2012) Adenosine A3 receptor is involved in ADP-induced microglial process extension and migration. *J Neurochem* 121(2):217–227.

47. Lanser AJ, et al. (2017) Disruption of the ATP/adenosine balance in CD39-/- mice is associated with handling-induced seizures. *Immunology* 152:589-601.

48. Sévigny J, et al. (2002) Differential catalytic properties and vascular topography of murine nucleoside triphosphate diphosphohydrolase 1 (NTPDase1) and NTPDase2 have implications for thromboregulation. *Blood* 99(8):2801–2809.
49. Robson SC, et al. (2005) Ectonucleotidases of CD39 family modulate vascular inflammation and thrombosis in transplantation. *Semin Thromb Hemost* 31(02):217–233.
50. Antonioli L, Pacher P, Vizi ES, Haskó G (2013) CD39 and CD73 in immunity and inflammation. *Trends Mol Med* 19(6):355–367.
51. Rymo SF, et al. (2011) A two-way communication between microglial cells and angiogenic sprouts regulates angiogenesis in aortic ring cultures. *PLoS ONE* 6(1):e15846.
52. Stankovic ND, Teodorczyk M, Ploen R, Zipp F, Schmidt MHH (2016) Microglia–blood vessel interactions: a double-edged sword in brain pathologies. *Acta Neuropathol (Berl)* 131(3):347–363.
53. Wu Y, et al. (2006) RanBPM associates with CD39 and modulates ecto-nucleotidase activity. *Biochem J* 396(1):23–30.
54. Woo JA, Roh S-E, Lakshmana MK, Kang DE (2012) Pivotal role of RanBP9 in integrin-dependent focal adhesion signaling and assembly. *FASEB J* 26(4):1672–1681.
55. Ohsawa K, et al. (2010) P2Y12 receptor-mediated integrin-β1 activation regulates microglial process extension induced by ATP. *Glia* 58(7):790–801.
56. Kim C, et al. (2014) β1-integrin-dependent migration of microglia in response to neuron-released α-synuclein. *Exp Mol Med* 46(4):e91.
57. Melani A, et al. (2012) Ecto-ATPase inhibition: ATP and adenosine release under physiological and ischemic in vivo conditions in the rat striatum. *Exp Neurol* 233(1):193–204.
58. Burnstock G (2006) Historical review: ATP as a neurotransmitter. *Trends Pharmacol Sci* 27(3):166–176.

59. Newman EA (2005) Calcium increases in retinal glial cells evoked by light-induced neuronal activity. *J Neurosci Off J Soc Neurosci* 25(23):5502–5510.
60. Kurth-Nelson ZL, Mishra A, Newman EA (2009) Spontaneous glial calcium waves in the retina develop over early adulthood. *J Neurosci* 29(36):11339–11346.
61. Gourine AV, et al. (2010) Astrocytes control breathing through pH-dependent release of ATP. *Science* 329(5991):571–575.
62. Vázquez C, et al. (2015) Endocannabinoids regulate the activity of astrocytic hemichannels and the microglial response against an injury: In vivo studies. *Neurobiol Dis*. 79:41-50.
63. Guthrie PB, et al. (1999) ATP released from astrocytes mediates glial calcium waves. *J Neurosci* 19(2):520–528.
64. Koizumi S, Fujishita K, Tsuda M, Shigemoto-Mogami Y, Inoue K (2003) Dynamic inhibition of excitatory synaptic transmission by astrocyte-derived ATP in hippocampal cultures. *Proc Natl Acad Sci U S A* 100(19):11023–11028.
65. Koizumi S, Fujishita K, Inoue K (2005) Regulation of cell-to-cell communication mediated by astrocytic ATP in the CNS. *Purinergic Signal* 1(3):211–217.
66. Zhang X, Chen Y, Wang C, Huang L-YM (2007) Neuronal somatic ATP release triggers neuron–satellite glial cell communication in dorsal root ganglia. *Proc Natl Acad Sci* 104(23):9864–9869.
67. Dibaj P, et al. (2010) NO mediates microglial response to acute spinal cord injury under ATP control in vivo. *Glia* 58(9):1133–1144.
68. Dibaj P, et al. (2010) Long-lasting post-mortem activity of spinal microglia in situ in mice. *J Neurosci Res* 88(11):2431–2440.
69. Dou Y, et al. (2012) Microglial migration mediated by ATP-induced ATP release from lysosomes. *Cell Res* 22(6):1022–1033.
70. Kim JV, Dustin ML (2006) Innate response to focal necrotic injury inside the blood-brain barrier. *J Immunol* 177(8):5269–5277.

71. Eyo UB, Miner SA, Ahlers KE, Wu L-J, Dailey ME (2013) $P2X_7$ receptor activation regulates microglial cell death during oxygen-glucose deprivation. *Neuropharmacology* 73:311–319.

72. Murana E, et al. (2017) ATP release during cell swelling activates a Ca^{2+}-dependent Cl^- current by autocrine mechanism in mouse hippocampal microglia. *Sci Rep.* 7(1):4184.

73. Bischofberger J, Engel D, Li L, Geiger JR, Jonas P (2006) Patch-clamp recording from mossy fiber terminals in hippocampal slices. *Nat Protoc* 1(4):2075–2081.

74. Kurpius D, Wilson N, Fuller L, Hoffman A, Dailey ME (2006) Early activation, motility, and homing of neonatal microglia to injured neurons does not require protein synthesis. *Glia* 54(1):58–70.

75. Gyoneva S, Traynelis SF (2013) Norepinephrine modulates the motility of resting and activated microglia via different adrenergic receptors. *J Biol Chem*.288(21):15291-15302.

76. Grinberg YY, Milton JG, Kraig RP (2011) Spreading depression sends microglia on Lévy flights. *PloS One* 6(4):e19294.

77. Hamilton NB, Kolodziejczyk K, Kougioumtzidou E, Attwell D (2016) Proton-gated Ca^{2+}-permeable TRP channels damage myelin in conditions mimicking ischaemia. *Nature* 529(7587):523–527.

78. Sholl DA (1953) Dendritic organization in the neurons of the visual and motor cortices of the cat. *J Anat* 87(Pt 4):387–406.1.

79. Wendt S, Wogram E, Korvers L, Kettenmann H (2016) Experimental cortical spreading depression induces NMDA receptor dependent potassium currents in microglia. *J Neurosci* 36(23):6165–6174.

80. Lopatin AN, Nichols CG (1996) $[K^+]$ dependence of polyamine-induced rectification in inward rectifier potassium channels (IRK1, Kir2.1). *J Gen Physiol* 108(2):105–113.

Figure Legends

Figure 1. Apyrase reduces microglial ramification and surveillance.

a-b Specimen images (left) and skeletonised arbours (right) of rat hippocampal microglia labelled with antibody to Iba-1 after superfusion with (**a**) control solution and (**b**) solution containing 200 U/ml apyrase (Sigma A7646). **c-e** 3D Sholl analysis derived values of number of process intersections with spherical shells at different distances from the soma (**c**, control and 200 U/ml curves differ significantly, p=0.0058), number of cell branch points (**d**), and number of process ends (**e**) for microglia in control solution or solution containing 100 or 200 U/ml apyrase. Number of cells on bars. **f-j** Effect of apyrase on microglial surveillance and ramification. **f** Colour coded superimposed images at 15 and 20 mins in control solution (top) and at 35 and 40 mins after starting apyrase superfusion at t=20 min (bottom; green, process extensions; red, process retractions; yellow, no change). **g-h** Plots of surveillance index (**g**) and ramification index (**h**) against time when individual microglia are exposed to apyrase (via a puffing pipette inserted into the slice). Control data (grey) show experiments with the puffing pipette filled with extracellular solution. **i-j** Surveillance index (**i**, see Materials and Methods) and ramification index (**j**) in control solution, and 100 and 200 U/ml apyrase. **k** Luciferin-luciferase luminescence (PMT current, arbitrary units, AU) evoked by ATP puff in control solution and solution containing apyrase (without a slice) illustrating that apyrase effectively degrades the puffed ATP (inset schematic shows experimental set-up, with blue showing the hippocampal stratum radiatum). **l** Mean luciferin-luciferase signal evoked by puffing 1 mM ATP onto a slice in the absence and presence of 100 U/ml apyrase (as in k), generated by a slice with no puffed ATP, and the baseline signal generated in the absence of a slice (con); inset shows records for the last two conditions with dashed line showing no signal.

Figure 2. Tonic ATP release does not maintain microglial surveillance & ramification.

a Current response of microglial cell clamped to 0 mV to puffed ATP (black boxes). Inset shows membrane potential response in an unclamped cell. **b-c** Inhibition of ecto-ATPases with ARL-67156 has no effect on microglial membrane potential (**b** specimen trace, **c** mean data, number of cells on bars). **d** Ecto-ATPase inhibition potentiates current response at 0 mV

to puffed ATP (black squares), but does not alter baseline current (red dashed line). **e** Mean normalised data for current evoked by puffed ATP in experiments like d, in the absence and presence of ARL-67156. **f-j** Effect of ecto-ATPase inhibition on microglial surveillance and ramification. **f** Colour coded superimposed images (as in Fig. 1f) at 5 and 10 mins in control solution (top) and at 35 and 40 mins (bottom) after starting ARL-67156 superfusion at t=20 min. (**g-h**) Time course of surveillance index (**g**) and ramification index (**h**) before and during superfusion of ARL-67156. **i-j** Mean normalised surveillance index (**i**) and ramification index (**j**) during superfusion of ARL-67156.

Figure 3. Apyrase depolarises microglia due to K^+ contamination.

a Microglial membrane potential depolarisation during superfusion of apyrase. **b** Mean membrane potential for microglia in control solution and in solution with 100 or 200 U/ml apyrase (Sigma A7646) added. Number of cells on bars; p values from t-tests are for comparison with control solution. **c** Effect of apyrase (Sigma A7646) on baseline membrane current at 0 mV of a microglial cell pulled out of the slice (apyrase evokes an inward current, shaded red) and on the response to puffed ATP (black squares, upward current deflections). **d** Specimen trace for measuring $[K^+]_e$ with a K^+-sensitive electrode in a slice during application of apyrase (Sigma A7646). **e** Mean $[K^+]_e$ measurements (as in d) when applying 100 U/ml apyrase (Sigma A7646) with no slice present or in a slice, or applying 200 U/ml apyrase to a slice. **f** $[K^+]_e$ measured with a blood gas analyser in extracellular solution to which different apyrase preparations were added at 100 U/ml (abscissa shows Sigma-Aldrich catalogue numbers); values include the 2.5 mM K^+ in the extracellular solution recipe. **g** Plot of $[K^+]_e$ (ordinate) in extracellular solution containing 100 U/ml apyrase made up from sources of different purity (abscissa). **h-l** Specimen images (left) and skeletonised arbours (right) of rat hippocampal slice microglia labelled with antibody to Iba-1 after incubation with (**h**) control solution and (**i**) solution containing 22.5 mM K^+ for 30 mins (see Materials and Methods for details). **j-l** Sholl analysis derived values of number of process intersections with spherical shells at different distances from the soma (**j**, control and 22.5 mM $[K^+]_e$ curves differ significantly, $p=2.4x10^{-4}$), number of cell branch points (**k**), and number of process ends (**l**) for

slices exposed to control solution or solution containing 22.5 mM $[K^+]_e$ (numbers of cells on bars). **m** Sholl analysis derived number of process ends (reflecting microglial ramification) after different times of exposure to 22.5 mM $[K^+]_e$ or 200 U/ml apyrase, and after 15 min washout, show a similar magnitude and time course of de-ramification and recovery for both conditions (p=0.68, 2-way ANOVA).

Figure 4. Dialysing apyrase retains microglial membrane potential and morphology.

a The luciferin-luciferase PMT signal evoked by puffing ATP in extracellular solution (without a slice) is reduced by the same amount by dialysed and undialysed apyrase. **b** Resting potential of microglia in normal extracellular solution (con), solution with 100 U/ml dialysed apyrase added (Sigma A7646), and solution with 100 U/ml undialysed apyrase added (as in Fig. 3b). Number of cells on bars. **c-e** Specimen images (left) and skeletonised arbours (right) of rat hippocampal slice microglia labelled with antibody to Iba-1 after incubation with (**c**) control solution, (**d**) solution containing dialysed apyrase (200 U/ml apyrase, Sigma A7646), and (**e**) solution containing non-dialysed apyrase. **f** 3D Sholl analysis derived values of number of process intersections with spherical shells at different distances from the soma for microglia superfused with solutions in c-e. Control and non-dialysed apyrase curves differ significantly, $p=2.9x10^{-3}$, whereas no difference exists between control and dialysed apyrase, p=0.91.

Figure 5. Regulation of adenine nucleotide levels and microglial membrane potential.

Left (green box): Tonic activity of K^+ channels generates a K^+ efflux (green arrow) which maintains the resting potential of microglia, which is essential for the normal ramification of microglia and hence their normal level of surveillance. Middle (red box): Tissue damage releases ATP. Endogenous ecto-ATPases on microglia and other brain cells hydrolyse ATP to ADP, and ADP to AMP (diagram shows ecto-ATPase only on microglia for simplicity). ADP, and possibly ATP, can activate $P2Y_{12}$ receptors on microglia. In the case of tissue damage this evokes process outgrowth (chemotaxis) to the damaged area. $P2Y_{12}$ activation also increases the activity of microglial K^+ channels (Fig. 2a), allowing $P2Y_{12}$ receptors to be used to sense the baseline level of ATP/ADP (as in Fig. 2). If there is tonic ATP release in physiological conditions, blocking ecto-ATPases with ARL-67156 will elevate extracellular

[ATP] and [ADP] and generate a membrane current. Figure 2d (baseline current) shows that no such current is generated, implying that there is no detectable tonic activation of $P2Y_{12}$ receptors. Right (blue box): Adding exogenous apyrase contaminated with K^+ raises $[K^+]_e$ artefactually and thus decreases the outward current through K^+ channels (shown as an inward shift of current: orange arrow), depolarising the microglia and decreasing ramification and surveillance. Adding apyrase (dialysed or undialysed) will also lower the extracellular level of ATP and ADP, as demonstrated in Figs. 1k and 4a.

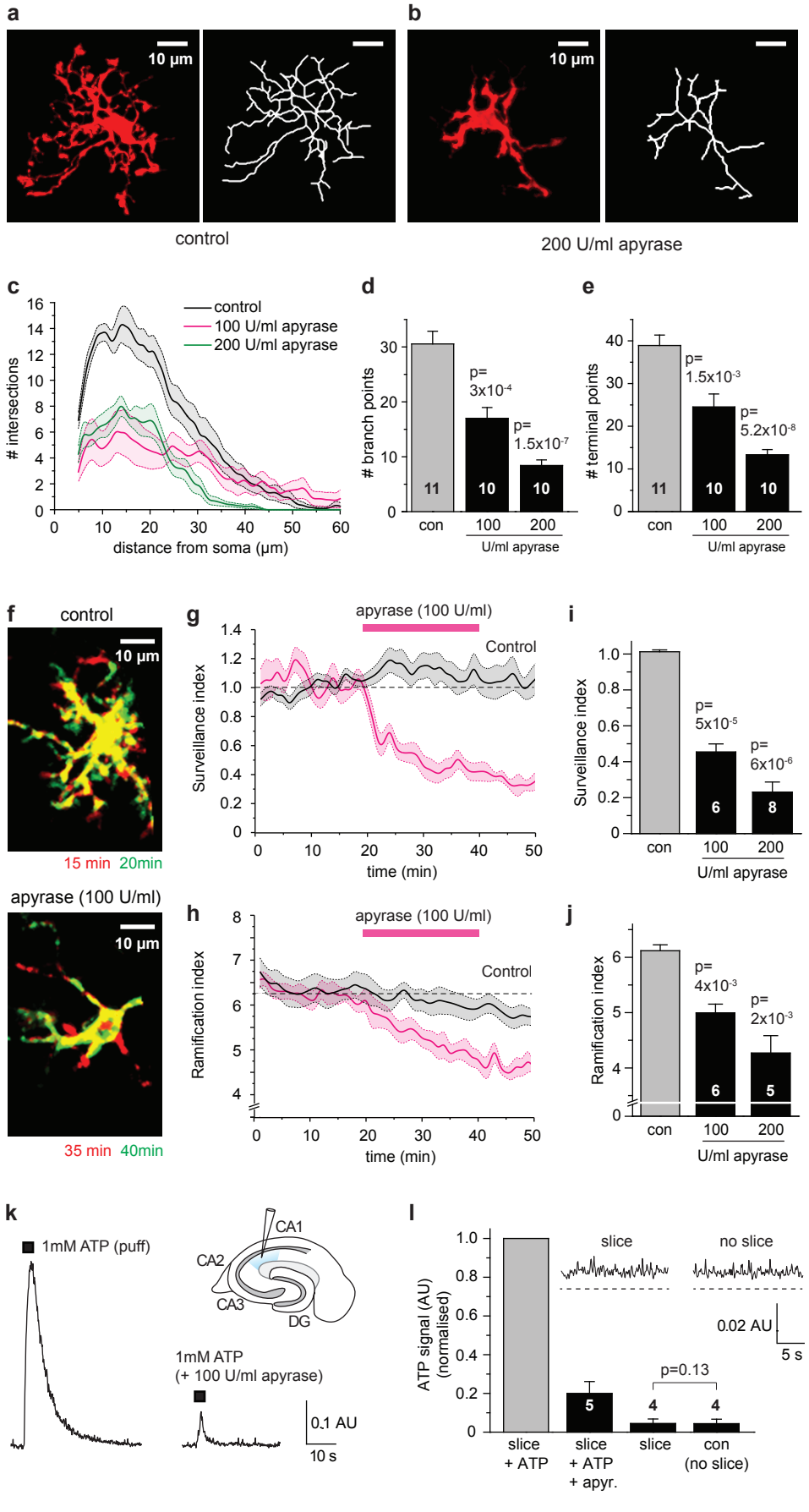
a
b
10 µm
control
200 U/ml apyrase
c
control
100 U/ml apyrase
200 U/ml apyrase
intersections
distance from soma (µm)
d
# branch points
p= 3x10-4
p= 1.5x10-7
11
10
10
con
100
200
U/ml apyrase
e
# terminal points
p= 1.5x10-3
p= 5.2x10-8
11
10
10
con
100
200
U/ml apyrase
f
control
10 µm
15 min 20min
apyrase (100 U/ml)
10 µm
35 min 40min
g
apyrase (100 U/ml)
Control
Surveillance index
time (min)
i
Surveillance index
p= 5x10-5
p= 6x10-6
6
8
con
100
200
U/ml apyrase
h
apyrase (100 U/ml)
Control
Ramification index
time (min)
j
Ramification index
p= 4x10-3
p= 2x10-3
6
5
con
100
200
U/ml apyrase
k
1mM ATP (puff)
CA1
CA2
CA3
DG
1mM ATP
(+ 100 U/ml apyrase)
0.1 AU
10 s
l
ATP signal (AU)
(normalised)
slice
no slice
0.02 AU
5 s
p=0.13
5
4
4
slice
+ ATP
slice
+ ATP
+ apyr.
slice
con
(no slice)

Fig. 1

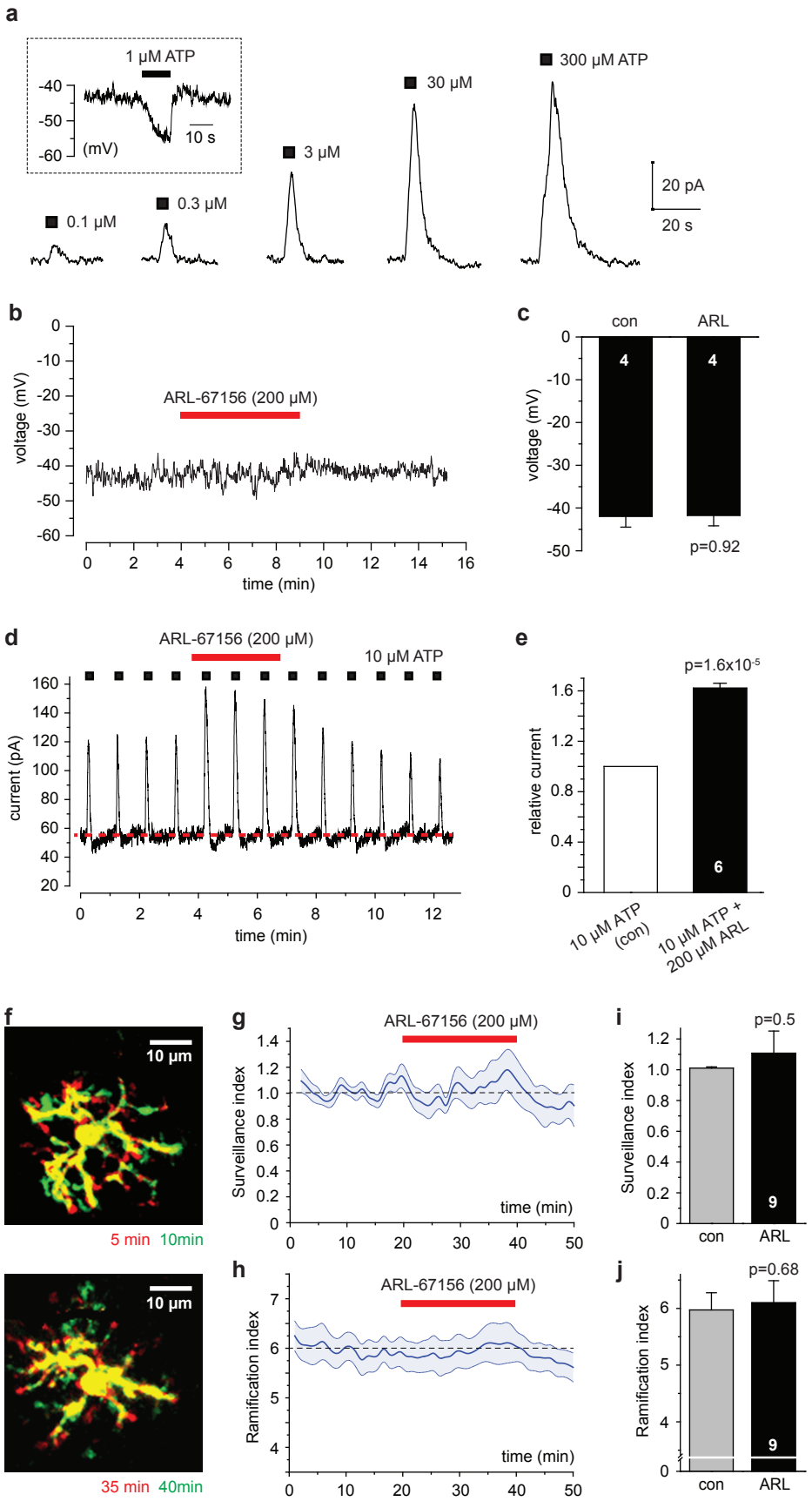
a
1 μM ATP
-40
-50
-60
(mV)
10 s
0.1 μM
0.3 μM
3 μM
30 μM
300 μM ATP
20 pA
20 s
b
voltage (mV)
ARL-67156 (200 μM)
time (min)
c
con
ARL
4
4
voltage (mV)
p=0.92
d
ARL-67156 (200 μM)
10 μM ATP
current (pA)
time (min)
e
p=1.6x10-5
relative current
6
10 μM ATP (con)
10 μM ATP + 200 μM ARL
f
10 μm
5 min 10min
10 μm
35 min 40min
g
ARL-67156 (200 μM)
Surveillance index
time (min)
h
ARL-67156 (200 μM)
Ramification index
time (min)
i
p=0.5
Surveillance index
9
con
ARL
j
p=0.68
Ramification index
9
con
ARL

Fig. 2

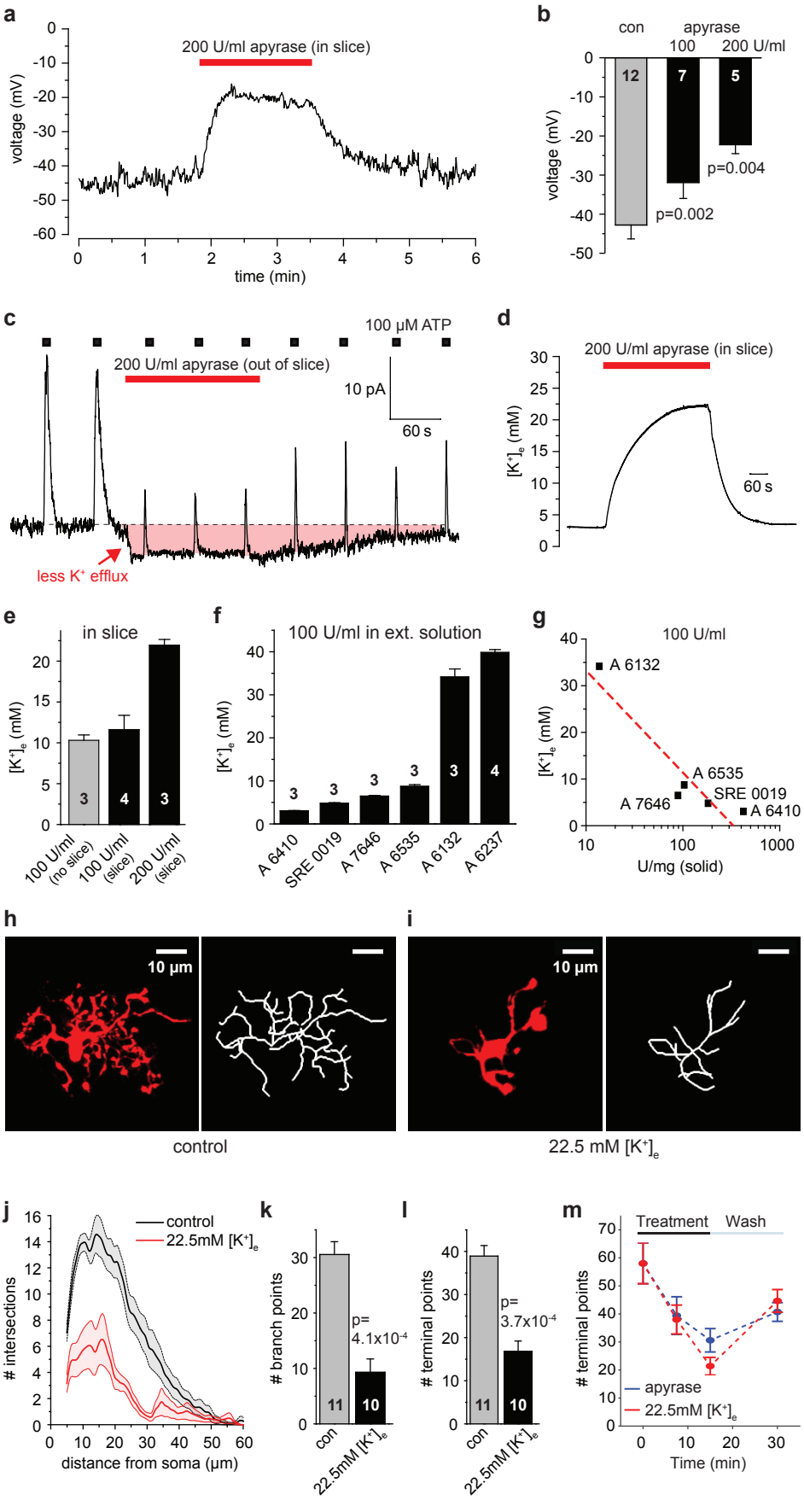
a
200 U/ml apyrase (in slice)
voltage (mV)
time (min)
b
con
apyrase
100
200 U/ml
12
7
5
p=0.002
p=0.004
voltage (mV)
c
100 µM ATP
200 U/ml apyrase (out of slice)
10 pA
60 s
less K+ efflux
d
200 U/ml apyrase (in slice)
[K+]e (mM)
60 s
e
in slice
[K+]e (mM)
100 U/ml (no slice)
100 U/ml (slice)
200 U/ml (slice)
f
100 U/ml in ext. solution
[K+]e (mM)
A 6410
SRE 0019
A 7646
A 6535
A 6132
A 6237
g
100 U/ml
A 6132
A 6535
SRE 0019
A 7646
A 6410
[K+]e (mM)
U/mg (solid)
h
10 µm
control
i
10 µm
22.5 mM [K+]e
j
control
22.5mM [K+]e
intersections
distance from soma (µm)
k
p= 4.1x10-4
# branch points
con
22.5mM [K+]e
l
p= 3.7x10-4
# terminal points
con
22.5mM [K+]e
m
Treatment
Wash
terminal points
apyrase
22.5mM [K+]e
Time (min)

Fig. 3

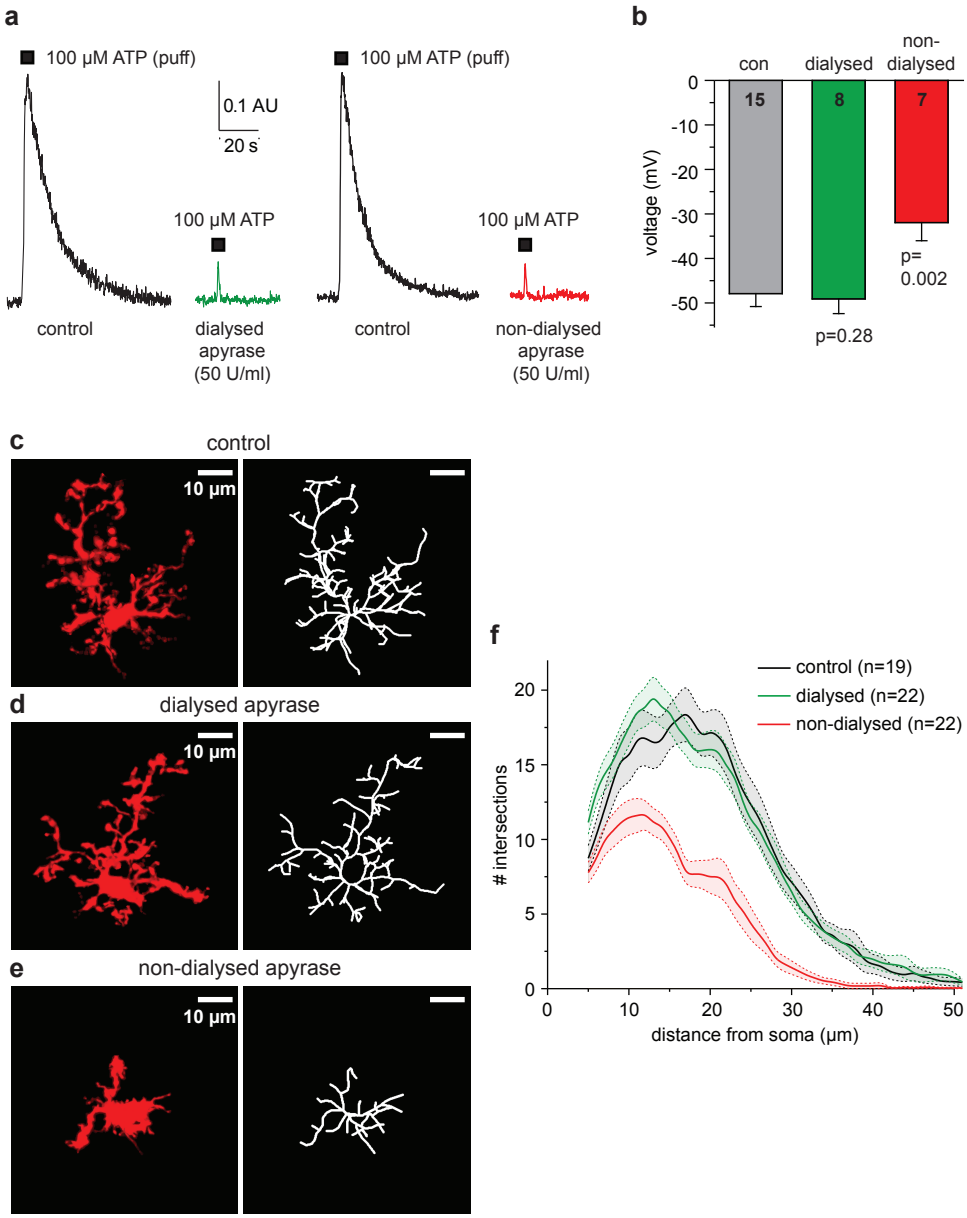
a
100 µM ATP (puff)
0.1 AU
20 s
100 µM ATP
control
dialysed apyrase (50 U/ml)
100 µM ATP (puff)
100 µM ATP
control
non-dialysed apyrase (50 U/ml)
b
con
dialysed
non-dialysed
15
8
7
voltage (mV)
0
-10
-20
-30
-40
-50
p=0.28
p= 0.002
c
control
10 µm
d
dialysed apyrase
10 µm
e
non-dialysed apyrase
10 µm
f
control (n=19)
dialysed (n=22)
non-dialysed (n=22)
intersections
0
5
10
15
20
0
10
20
30
40
50
distance from soma (µm)

Fig. 4

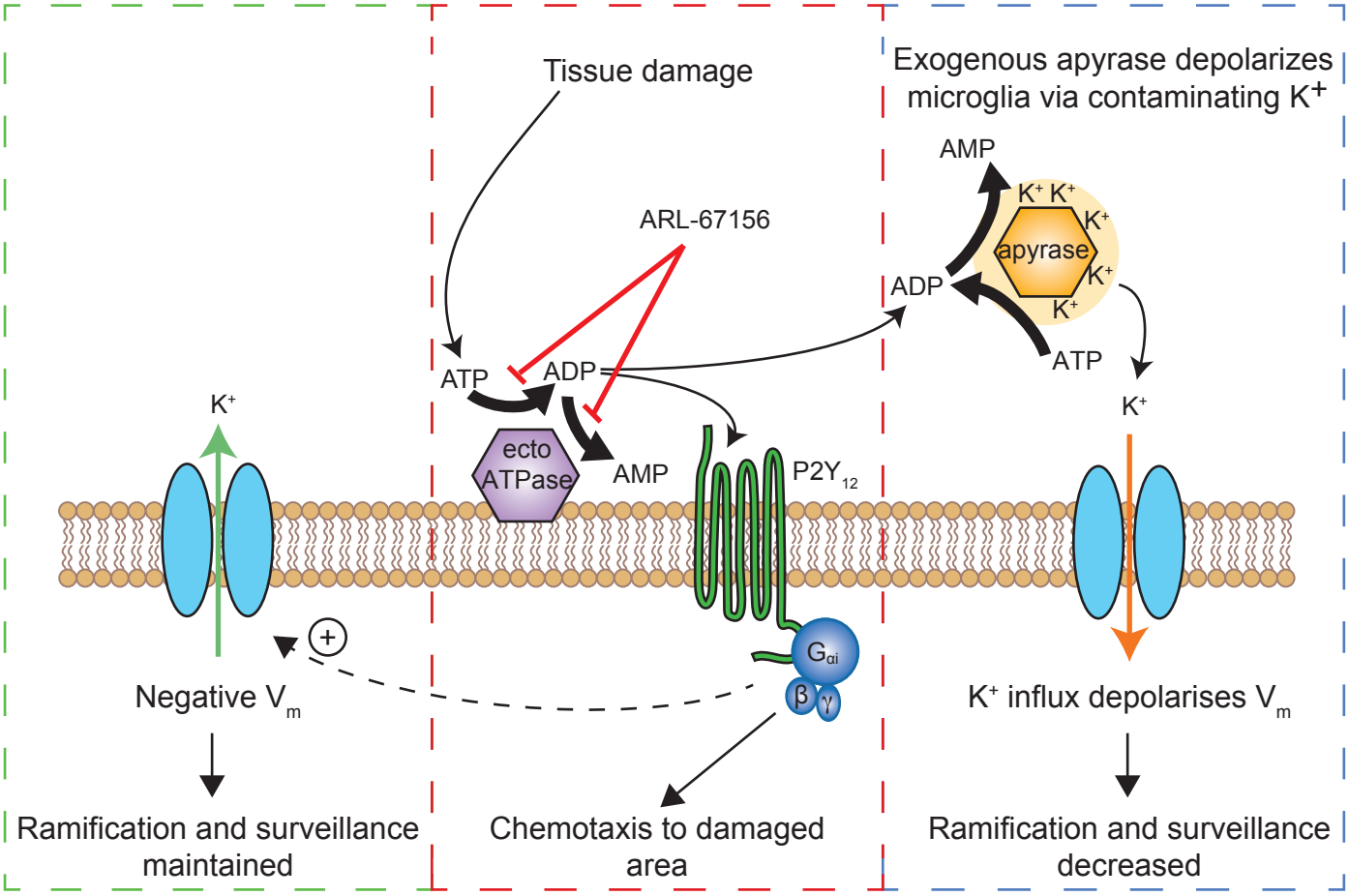
Tissue damage
Exogenous apyrase depolarizes microglia via contaminating K+
ARL-67156
AMP
K+ K+
K+
apyrase
K+
ADP
K+
ATP
ATP
ADP
K+
ecto ATPase
AMP
P2Y12
K+
Gαi
β γ
+
Negative Vm
K+ influx depolarises Vm
Ramification and surveillance maintained
Chemotaxis to damaged area
Ramification and surveillance decreased

Fig. 5

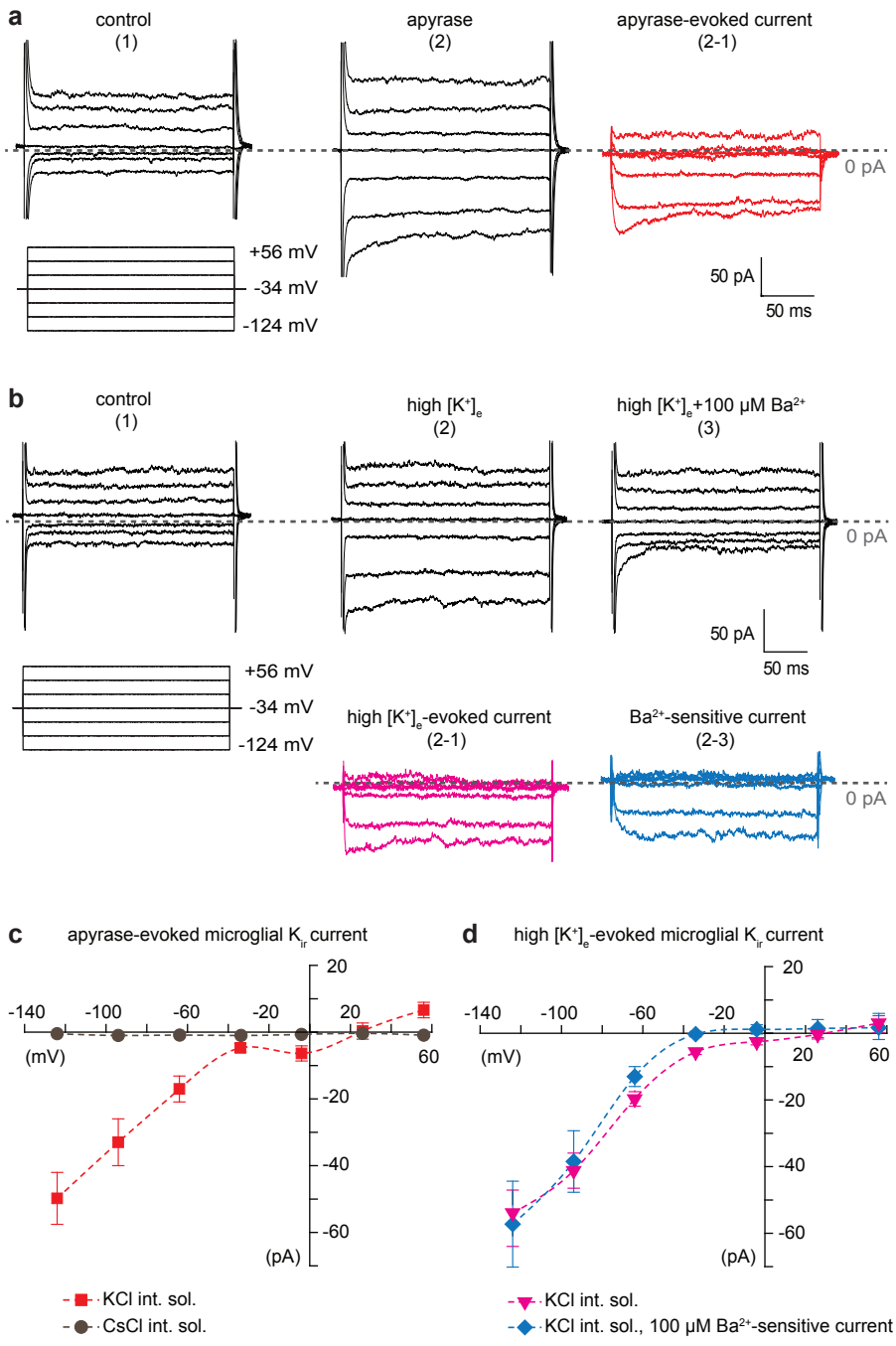
a
control
(1)
apyrase
(2)
apyrase-evoked current
(2-1)
0 pA
+56 mV
-34 mV
-124 mV
50 pA
50 ms
b
control
(1)
high [K+]e
(2)
high [K+]e+100 µM Ba2+
(3)
0 pA
50 pA
50 ms
+56 mV
-34 mV
-124 mV
high [K+]e-evoked current
(2-1)
Ba2+-sensitive current
(2-3)
0 pA
c
apyrase-evoked microglial Kir current
20
-140
-100
-60
-20
20
(mV)
60
-20
-40
-60
(pA)
KCl int. sol.
CsCl int. sol.
d
high [K+]e-evoked microglial Kir current
20
-140
-100
-60
-20
(mV)
20
60
-20
-40
-60
(pA)
KCl int. sol.
KCl int. sol., 100 µM Ba2+-sensitive current

Supp. Fig. 1

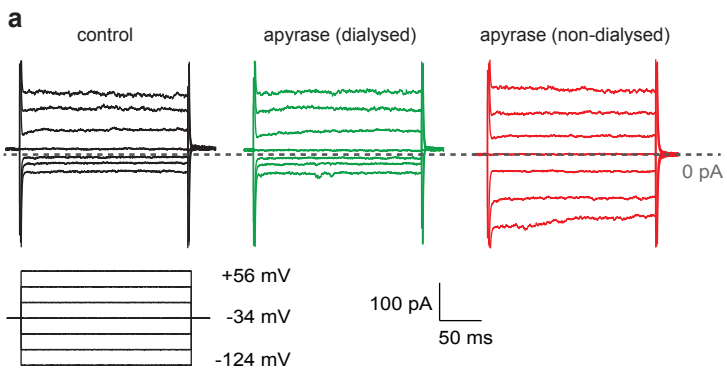
a
control
apyrase (dialysed)
apyrase (non-dialysed)
0 pA
+56 mV
-34 mV
-124 mV
100 pA
50 ms

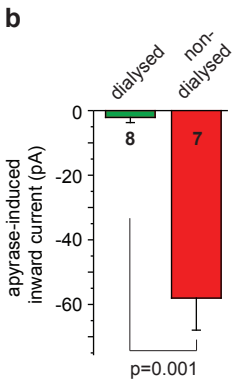
b
dialysed
non-dialysed
0
-20
-40
-60
apyrase-induced inward current (pA)
8
7
p=0.001

Supp. Fig. 2